

Superparamagnetic fluorescent nickel–enzyme nanobioconjugates: synthesis and characterization of a novel multifunctional biological probe†

Pramod Kumar Verma,^a Anupam Giri,^a Nguyen T. K. Thanh,^{*bc} Le Duc Tung,^b Oindrila Mondal,^d Mrinal Pal^d and Samir Kumar Pal^{*a}

Received 10th December 2009, Accepted 8th February 2010

First published as an Advance Article on the web 10th March 2010

DOI: 10.1039/b925477c

We report, for the first time, the synthesis of superparamagnetic and fluorescent nickel (Ni) nanoparticles (consisting of a single material) directly conjugated to an enzyme, bovine pancreatic α -chymotrypsin (CHT), by chemical reduction in aqueous solution. The structural characterization of Ni–CHT nanobioconjugates was carried out using UV-VIS absorption/photoluminescence spectroscopy and high-resolution transmission electron microscopy. The temperature dependence of the magnetization $M(T)$ taken in zero field cooling and field cooling conditions, exhibits the main features of superparamagnetism. Circular dichroism studies were performed to monitor the structural perturbation to the structure of the enzyme after conjugation with the nickel nanoparticles (Ni NPs). The functional integrity of the enzyme conjugated to the Ni NPs was investigated by monitoring the enzymatic activity of the Ni–CHT conjugates using UV-VIS absorption spectroscopy and comparison with the unbound enzyme under similar experimental conditions. To confirm the conjugation of Ni NPs to CHT, we carried out Förster resonance energy transfer (FRET) studies using a fluorescent probe, 4-nitrophenyl anthranilate (NPA), known to bind at the enzymatic active site of CHT, as the donor (D) and Ni-NP-bound CHT as the acceptor (A). Our studies also demonstrated that the FRET from the donor NPA to the acceptor Ni NPs in CHT can be monitored to follow the D–A distance and hence the protein structure during thermal unfolding. Such a multifunctional superparamagnetic, fluorescent and biologically active nanobioconjugate may be of relevance in nanoparticle-based diagnostic and therapeutic applications.

Introduction

Biological systems form sophisticated mesoscopic and macroscopic structures with tremendous control over the placement of nanoscopic building blocks within extended architectures. Both biological and nanoscale science meet at the same length scale because biomolecular components have typical size dimensions in the range of about 2–100 nm. In this regard, synthesis of bioconjugate nanoparticles using biological macromolecules^{1,2} has recently aroused great interest due to the broad range of applications of such hybrid materials, from life sciences to materials and nanosciences. The motivation is based on the unique properties of nanoparticles possessing strongly size-

dependent optical, electrical, magnetic, and electrochemical properties combined with the perfect binding and biochemical functionality of biomacromolecules. Examples of biotemplate synthesis of metal nanoparticles include the binding of metal ions to surface layer proteins,³ DNA,⁴ virus protein cages,⁵ or ordered protein assemblies⁶ to initiate sites of nucleation for nanoparticle growth and the synthesis of metallic nanocrystals through the use of amino acids as capping and reducing agents in an aqueous medium.⁷

Metal nanoparticles (which have sizes comparable to the Fermi wavelength of an electron, exhibit molecule-like behavior including discrete electronic states and size-dependent fluorescence^{8,9} due to quantum size effects) as fluorescent probes have found increased applications for cell labeling,¹⁰ biological labeling,¹¹ biological detection,¹² and *in vivo* imaging.^{13,14} Magnetic nanoparticles, such as superparamagnetic iron oxide particles, have been extensively used in biological applications, such as magnetic resonance imaging (MRI) contrast enhancement, hyperthermia treatment, and gene and drug delivery.^{15–19} Owing to their small size and high surface area, magnetic nanoparticles respond well to magnetic control, which has led to several successful applications such as in tissue repair, immunoassays, detoxification of biological fluids,²⁰ bacteria detection²¹ and separation and purification of cells and biomolecules in bioprocesses.^{22–24} Combining the fluorescence and magnetic properties into a nanosphere of a single material would lead to new applications in biological systems^{25,26} and hence the

^aUnit for Nano Science & Technology, Department of Chemical, Biological & Macromolecular Sciences, S.N. Bose National Center for Basic Sciences, Block JD, Sector III, Salt Lake, Kolkata 700098, India. E-mail: skpal@bose.res.in

^bThe Davy-Faraday Research Laboratory, The Royal Institution of Great Britain, 21 Albemarle Street, London, UK W1S 4BS

^cDepartment of Physics and Astronomy, University College London, Gower Street, London, UK WC1E 6BT. E-mail: ntk.thanh@ucl.ac.uk; Fax: +44 (0) 207-629-3569; Tel: +44 (0) 207-491-6509

^dDepartment of Physics, The University of Burdwan, Golapbag, Burdwan 713104, West-Bengal, India

† Electronic supplementary information (ESI) available: Details of steady-state measurements, time-resolved measurements, DA distance measurements from FRET, and calculation of molar extinction coefficients of NP solutions from theoretical considerations. See DOI: 10.1039/b925477c

synthesis of such nanoparticles has, in particular, captured the growing interests of research at the interfaces of chemistry, physics, biology, and materials science. There have been a few reports on the preparation of such bifunctional nanocrystals using quantum dots (QDs) and magnetic nanoparticles. Wang for the first time synthesized a bifunctional water-soluble nanocomposite consisting of a magnetic core and luminescent QD shell (CdSe/ZnS) and used it to separate and detect breast cancer cells in serum.²⁵ Gu *et al.* reported a method for generating heterodimers of FePt@CdS core-shell nanoparticles by taking advantage of lattice mismatching and selective annealing at a relatively low temperature.²⁷ Recently Gao *et al.* demonstrated the intracellular manipulation of fluorescent magnetic Fe₃O₄-CdSe nanoparticles using a small magnet.²⁸ All the above mentioned bifunctional nanoparticles used QDs as luminescent probes and magnetic nanoparticles. Now the question is whether one can prepare a luminescent and magnetic nanoparticle consisting of a nanoparticle with a single material instead of a composite nanoparticle system?

In the present work, we have synthesized, for the first time, luminescent and magnetic Ni NPs of 2.5 nm average diameter consisting of a single material instead of a composite nanoparticle system using an enzyme, bovine pancreatic α -chymotrypsin (CHT). We obtain well-dispersed, protein-nickel NPs that remain stable indefinitely in solution without any aggregation or deterioration of the spectral properties. The structural characterization of CHT encapsulated Ni NPs was done using steady-state UV-VIS absorption/photoluminescence (PL) spectroscopy and high resolution transmission electron microscopy (HRTEM). A comparative study on the enzymatic activity of the nanobioconjugates with the unbound enzyme, under similar experimental conditions, was also done. Picosecond-resolved FRET from a fluorescent probe at the enzymatic active site to the Ni NPs in the nanobioconjugates reveals the possible location of the metal cluster in CHT. We also explored the possibility of using the FRET to monitor various temperature-induced unfolding states of the enzyme CHT. The synthesis methodology followed here is simpler compared to those of composite bifunctional NPs which may be extended further to Co, Fe *etc.* The combination of fluorescent and magnetic properties in one material would allow for visualization by fluorescence and manipulation in magnetic fields and could potentially be exploited for biomedical applications (*e.g.*, magnetic separation, immunoassays, stem cell tracking, cancer metastasis monitoring using MRI, targeted drug delivery and hyperthermia cancer treatment).

Results and discussion

Fig. 1a presents the TEM image of a dialyzed sample of Ni-CHT nanobioconjugates. The image reveals that the nanobioconjugates are almost spherical in shape and follow a uniform size distribution. Particle sizes have been estimated by fitting our experimental data measured from the TEM image, with a log-normal size distribution. The size distribution is shown as an inset in Fig. 1a. The average size of the Ni particles, as estimated from the TEM image, has been found to be 2.5 nm. The corresponding HRTEM image (Fig. 1b) confirms the crystallinity of these NPs in their structure. The interplanar distance of

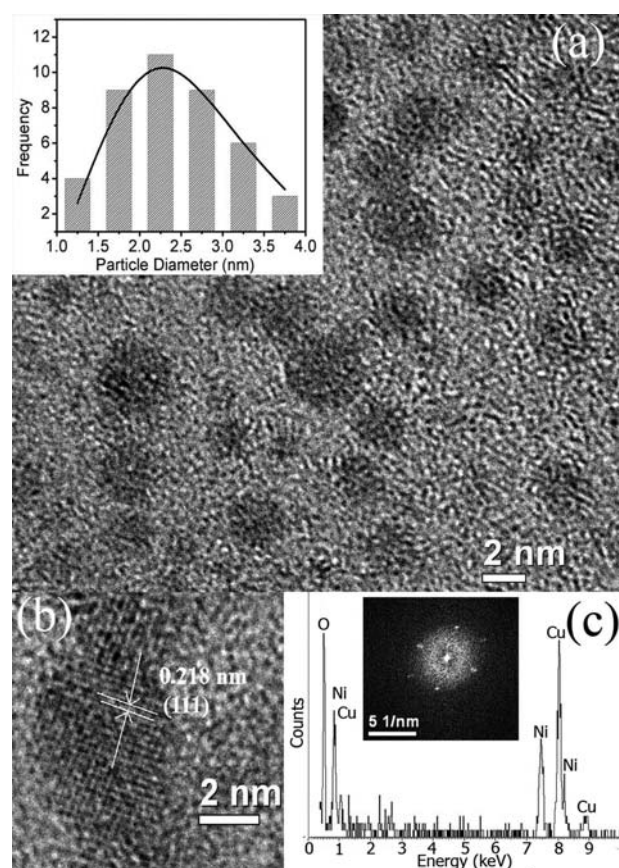


Fig. 1 (a) TEM image of as-prepared dialyzed Ni-CHT nanobioconjugates. The size distribution of the sample is shown in the inset. (b) A HRTEM image showing the crystalline structure of Ni NPs. (c) EDAX spectrum of the Ni NPs. Ni peaks at 0.9, 7.5 and 8.3 keV. An FFT image of the Ni-CHT nanobioconjugate is shown in the inset.

the fringes is measured to be about 0.218 nm, corresponding to the distance between the (111) planes of the nickel crystal lattice. The image in the inset of Fig. 1c represents the corresponding fast Fourier transform (FFT) pattern. It has to be noted that the average size of 2.5 nm Ni NPs obtained in the dialyzed sample, which is confirmed from TEM and absorption studies (see later in the text), cannot be formed from free Ni ions because of the unavailability of any stabilizing agent to control their size. Thus in our experimental conditions, the possibility of formation of free larger Ni nanoparticles of micrometre size (due to uncontrolled growth) is negligibly small as they are not revealed in the TEM images of the dialyzed sample. A typical energy-dispersive X-ray (EDAX) spectrum of a dialyzed Ni-CHT sample is shown in Fig. 1c and demonstrates the presence of Ni.

It is well known that the optical properties of metal nanoparticles are caused by surface plasmons. The most famous surface plasmonic nanoparticles are ones of noble metals such as gold, silver²⁹ and copper³⁰ in the visible region. There are few reports on the optical properties of Ni (transition metal) nanoparticles in sol-gel films³¹ and silica glass.³²⁻³⁴ Recently Yeshchenko *et al.* reported the surface plasmon resonance (SPR) band of Ni NPs in SiO₂ glass at 358–382 nm depending on the annealing conditions.³⁴ The inset of Fig. 2b shows the UV-Vis absorption spectrum of Ni-CHT conjugates, which reveals

a surface plasmon band located at 417 nm. On the basis of Mie theory³⁵ and its generalized versions,^{36,37} information concerning Ni nanoparticle sizes can be derived from the analysis of the absorption band. The linear optical absorption coefficient, $\sigma(\lambda)$, of a collection of uniform metallic spheres whose dimensions are very small compared to the wavelength of the incident light is well described by Mie scattering theory in the electric dipole approximation and is given by:

$$\sigma(\lambda) = \left(\frac{18\pi V \varepsilon_m^{3/2}}{\lambda} \right) \frac{\varepsilon''(\omega)}{(\varepsilon'(\omega) + 2\varepsilon_m)^2 + \varepsilon''(\omega)^2} \quad (1)$$

where λ is the incident wavelength with a corresponding frequency ω , V is the volume of the spherical particle (*i.e.*, $4\pi r^3/3$), ε_m is the dielectric constant of the medium, and $\varepsilon'(\omega)$ and $\varepsilon''(\omega)$ are the real and the imaginary parts of the dielectric constant of the metal. The absorption coefficient in eqn (1) has a maximum value at the SPR frequency, when $\varepsilon'(\omega) + 2\varepsilon_m = 0$, the peak wavelength of the band depending on the dielectric constants of the medium and the metal particles.

The average radius of the Ni NPs (assumed to be spherical), small compared to the wavelength of light, can be approximately estimated from the resonance optical absorption spectrum as per the Mie scattering formula:

$$r_{\text{metal}} = \frac{v_F}{\Delta\omega_{1/2}} = \frac{v_F}{2\pi c_0 \left(\frac{\Delta\lambda}{\lambda_P^2} \right)} \quad (2)$$

where v_F is the Fermi velocity (2.33×10^6 m s⁻¹ for Ni)³⁸ and $\Delta\omega_{1/2}$ is the full width at half-maximum (FWHM) of the SPR absorption when plotted as a function of angular frequency ω , c_0 is the speed of light in vacuum, λ_P is the wavelength where the absorption peak appears, and $\Delta\lambda$ gives the FWHM of the band. The average radius of the NPs calculated using eqn (2) is found to be in the range of 2.8 nm, consistent with the size obtained from the TEM image. The Ni-CHT nanobioconjugates exhibited fluorescence in the visible region, as shown in Fig. 2a. The photoluminescence of the nanoparticles arises due to their molecule-like electronic structure. The origin of the emission is not very clear at this moment compared to other Ni-based nanoparticles reported in the literature,^{34,39} however, it could be due to the recombination of the excited electrons from excited states in the sp band with the holes in the low-lying d band (interband transition). Fluorescence decay of the Ni-CHT nanobioconjugates was measured. Data obtained using a picosecond-resolved time-correlated single-photon counting (TCSPC) technique are shown in Fig. 2b. Lifetime values of the Ni-CHT nanobioconjugates were obtained by the numerical fitting of the fluorescence at 500 nm. They are 0.12 ns (54.3%), 1.17 ns (17.4%) and 4.34 ns (28.3%). The overall PL decay leads to an average lifetime value of 1.49 ns. It is important to note that the excitation spectra of Ni-CHT nanobioconjugates show peaks centered at 320 nm and 360 nm (Fig. 2a). So the conclusion is that the SPR peak centered at 417 nm is not responsible for the luminescence. It has been demonstrated previously⁴⁰ for spherical NPs that the broadening of the plasmon with decreasing size in the quantum size regime, $d < 3$ nm, in the case of both Au and Ag is rapid and increases the absorbance of both UV and NIR regions relative to the plasmon peak, whose intensity decreases instead. It is in fact well established that the surface plasmon bandwidth is inversely proportional to the radius r of the particle for sizes smaller than about 20 nm.⁴¹ The increased broadening with decreasing size enhances both the low- and high-energy absorbance of the smallest clusters, causing the plasmon to be completely damped below a size of $d = 2.2$ nm for Au but still observable at a size of $d = 1.55$ nm for Ag.⁴⁰ In our case the emitting Ni NPs (conjugated to CHT) are smaller than the 2.5 nm and their SPR is not observable in the absorbance spectra due to broadening as explained above.

Magnetic properties of the Ni NPs were studied by using standard zero-field-cooling (ZFC) and field-cooling (FC) procedures and field-dependent magnetization measurements. Measurements of the ZFC, FC magnetization as a function of temperature were performed between 5 K and 300 K under an applied field of 100 Oe and the results are shown in Fig. 3a. The ZFC/FC curve evidences a superparamagnetic behavior above the blocking temperature $T_B = 13.2$ K. Here, T_B is determined from the peak of the ZFC curve above which the magnetic anisotropy energy barrier of the nanoparticle is overcome by thermal activation and the nanoparticle becomes superparamagnetically relaxed. Superparamagnetic relaxation is an essential requirement for the magnetic nanoparticles to be used

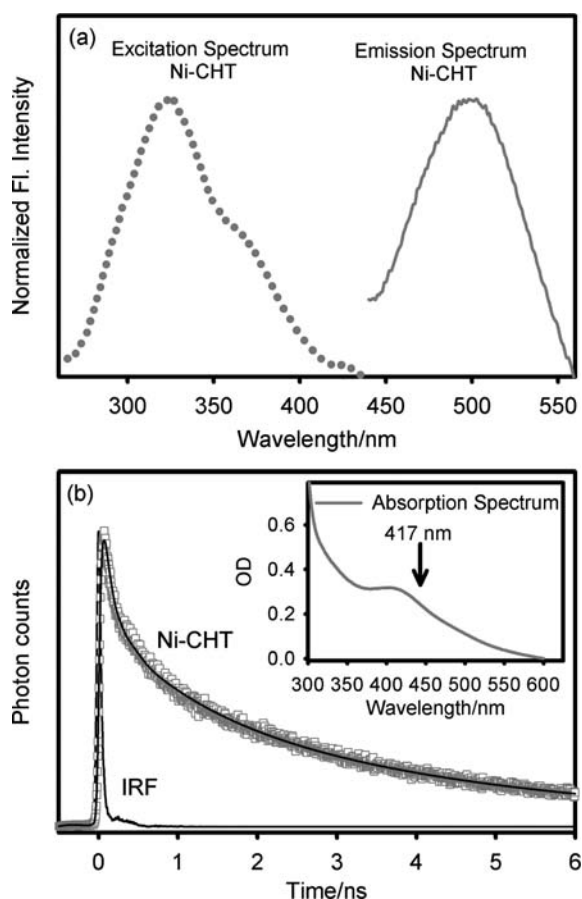


Fig. 2 (a) Excitation and emission spectra of Ni-CHT nanobioconjugates. (b) Fluorescence decay of Ni-CHT nanobioconjugate ($\lambda_{\text{ex}} = 375$ Å) monitored at 500 nm. The absorbance spectrum of Ni-CHT nanobioconjugates is shown in the inset. IRF stands for instrument response function.

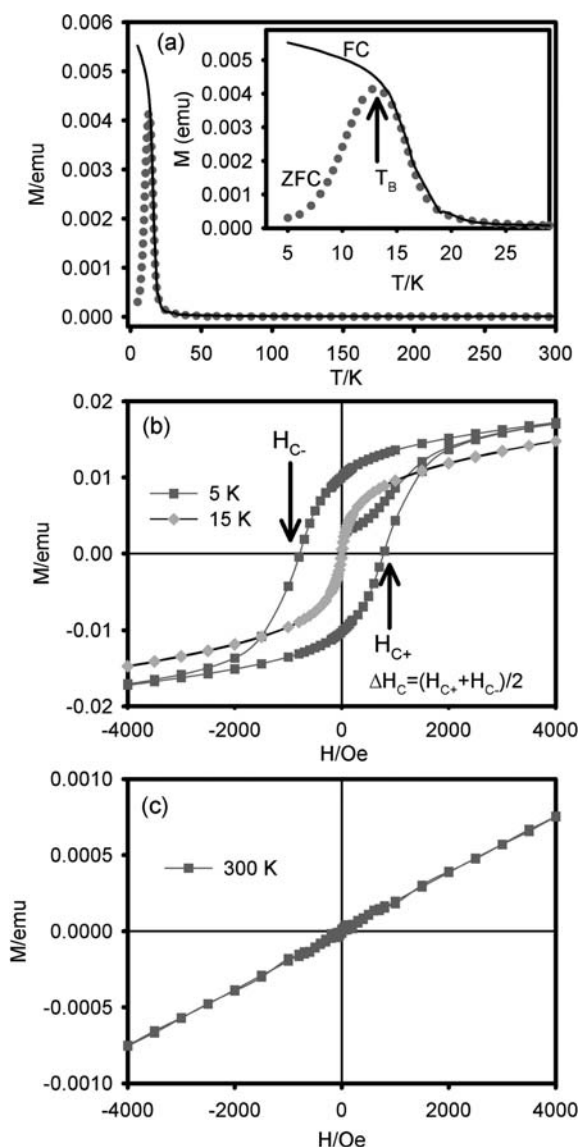


Fig. 3 (a) ZFC and FC magnetization as a function of temperature measured at an applied field of 100 Oe for the Ni-CHT nanobioconjugates. Inset: an expanded view of the plot, clearly showing T_B . (b) M - H plots of Ni NPs at 5 K (symbol: square) and 15 K (symbol: diamond). (c) M - H plot at 300 K of the Ni-CHT nanobioconjugates.

as contrast agents for MRI. Below T_B the sample is seen as a stable ferromagnet which is manifested by the observation of the hysteresis in the M versus H plot at 5 K (Fig. 3b) with a coercivity (H_C) of around 800 Oe. The 5 K hysteresis loops are symmetric about zero field ($\Delta H_C \sim 0.5$ Oe) suggesting the absence of an antiferromagnetic NiO layer on the surfaces of the Ni NPs.⁴² The $M(H)$ curve at room temperature (Fig. 3c) shows a linear behaviour with low magnetization values, indicative of superparamagnetic behaviour, with zero coercivity (H_C) and remanent magnetization. This is related to the fine crystallite sizes of the Ni particles which are in the nanometre range. Previous works on Ni NPs reported values of the blocking temperature ranging from 18 K to 40 K.⁴²⁻⁴⁴ For superparamagnetic particles,⁴⁵ $T_B = KV/25k_B$ where K denotes the magnetic anisotropy constant, k_B is the Boltzmann constant, and

V is the volume of particles. For magnetic NPs with 2.5 nm, the anisotropy is found to be 6.96×10^5 erg cm^{-3} . When all of the nanoparticles are at the superparamagnetic relaxation state above T_B , their magnetization decreases with increasing temperature and it follows the Curie-Weiss law. The computed value of the magnetic moment from the ZFC curve by applying Curie-Weiss C/T law is found to be $0.49 \mu_B$ which is slightly lower than $0.54 \mu_B$ for the theoretical value of the atomic moment of Ni metal.

It is well-known that sodium borohydride induces cleavage of disulfide bonds to sulfhydryl groups in a protein and perhaps also breaks some of the peptide bonds leading to its denaturation. Reconstitution of a protein denotes the process of returning a denatured protein to its original structure and activity. In our experiment, CHT and Ni-CHT conjugates were reconstituted by dialyzing each of them separately against water of pH = 8.0-8.5 for 24 h in aerated conditions. Fig. 4 compares the circular dichroism (CD) spectra of reconstituted CHT and reconstituted Ni-CHT solutions. Native CHT displays CD features with minima at 202 and 232 nm, corresponding to the native secondary and tertiary structures of the protein,^{46,47} respectively. It is found that there is a slight loss of tertiary structure in the CD spectrum at 232 nm and a ~ 3 nm shift of the minimum at 202 nm for both reconstituted CHT as well as reconstituted Ni-CHT samples compared to the native CHT. Quantification of the CD data through curve-fitting analysis revealed that the conformation of the reconstituted Ni-CHT (19% helix) was identical to that of the reconstituted CHT (19% helix), demonstrating a small perturbation of the native structure of the protein (24% helix).

To prove that the Ni-bound CHT NPs are still functional, we also measured the enzymatic activity of Ni-CHT and the results are shown in the inset of Fig. 4. We found that the specific activity (in units/mg) of the reconstituted Ni-CHT complex was retarded by 2 times compared to that of reconstituted CHT, consistent with our previous studies^{48,49} on analogous systems (CdS-bound CHT and Ag-bound CHT). Our observation also closely matches the enzymatic activities performed by Jordan *et al.*⁴⁷ for a similar system (CHT-Au-TCOOH; Au-TCOOH being gold-nanoparticle-capped tetra(ethylene glycol)

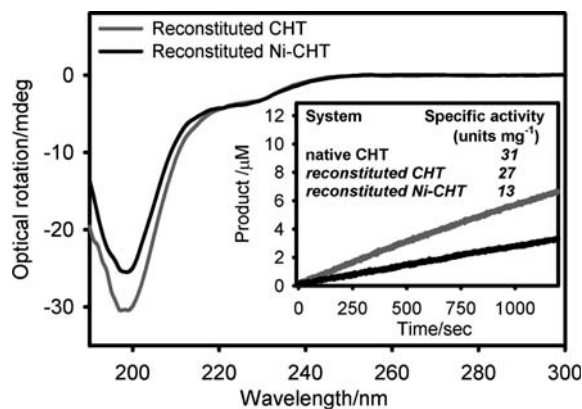


Fig. 4 CD spectra of reconstituted CHT and reconstituted Ni-CHT nanobioconjugates. Inset: enzymatic activities of CHT and reconstituted Ni-CHT nanobioconjugates on the substrate, AAF-AMC.

carboxylate ligands) where they observed a 3-fold decrease in the rate of CHT complexed with Au-TCOOH compared to CHT alone. The above experimental observations may indicate that the nucleation and subsequent growth of Ni NPs in CHT could possibly take place at a site that is away from the enzymatic active site of CHT. It has to be noted that the attachment of a 2.5 nm diameter NP to the active site of the enzyme is expected to act as an inhibitor of CHT activity on the substrate AAF-AMC (1–2 nm diameter) resulting in retardation of the enzymatic activity by several orders of magnitude.⁵⁰ However, the moderate retardation in the enzymatic activity of Ni-CHT complexes as compared to CHT alone could be the manifestation of the dynamic rigidity of CHT upon attachment of a Ni NP.

The enzyme α -CHT, isolated from bovine pancreas, belongs to a class of digestive serine proteases, and has the biological function of hydrolyzing polypeptide chains. It is well-known from the crystalline structure of α -CHT that it has a total of 5 disulfide bonds and 2 histidine groups (protein data bank, ID code 2CHA). Imidazole-N donor atoms of histidine and thiol sulfur atoms of cysteine are the most common metal-binding sites in proteins. Nickel has a high affinity for sulfur; cysteine has three potential donor atoms: carboxyl, sulfhydryl and amino acids, of which only the latter two are coordinated, leaving the carboxyl group unbound.^{51–53} Histidine generally binds nickel through heterocyclic nitrogen. Out of five disulfides, two (Cys1–Cys122 and Cys42–Cys58) are close (within 8 Å) to the enzymatic active site. The three remaining disulfide bonds (Cys191–Cys220, Cys136–Cys201 and Cys168–Cys182) are away from enzymatic site. One of two histidines, His57, is present in the active site of the enzyme (a catalytic triad comprising the residues His57, Ser195, and Asp102) and the other (His40) is 16 Å away from His57. From the enzymatic activity studies, we found only slight retardation of the activity of reconstituted Ni-CHT compared to reconstituted CHT and hence this rules out the possibility of the His57 and disulfide bond close to the enzymatic center for the formation of the nanobioconjugates. The possibility of the formation of Ni NPs in CHT through His40 is also ruled out because FRET studies (see later text) revealed that the nucleation site is at least ~ 30 Å (the distance between His57 and His40 is found to be 15.82 Å) away from the catalytic triad. So the remaining 3 disulfide bonds are possible sites of nucleation of the Ni NPs.

The interaction of Ni(II) with terminal amino groups and adjacent peptide nitrogen atoms has also been postulated with lysine, conalbumin, ribonuclease, vasopressin and α -CHT.⁵⁴ To confirm the conjugation of Ni NPs to CHT possibly *via* amines/thiols present in different residues, we carried out FRET studies using a fluorescent probe, NPA, known to bind at the enzymatic active site⁵⁵ of CHT as the donor with Ni NPs as the acceptor. The spectral overlap between NPA-CHT emission and the absorption of Ni-CHT NPs is expected to reveal interprobe distance, when they are in a close proximity. Fig. 5a reveals the significant spectral overlap between the NPA-CHT emission spectrum (donor D, emission maximum at 428 nm) and the Ni-CHT absorption spectrum (acceptor A, absorption maximum at 417 nm) that favors the energy transfer from NPA to Ni in CHT. The molar extinction coefficient of Ni-CHT conjugates required for energy transfer calculations was computed from theoretical considerations using the maximum absorbance value of the SPR

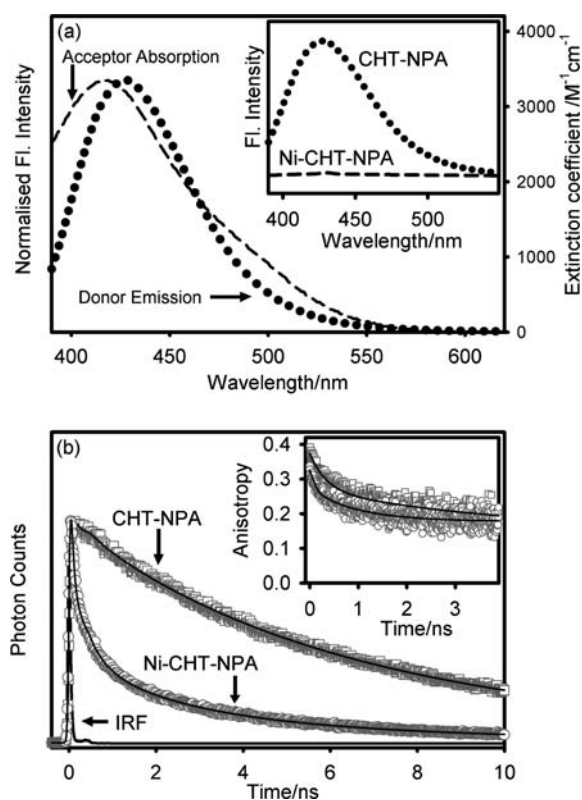


Fig. 5 (a) Spectral overlap between donor (NPA-CHT) emission and acceptor (Ni-CHT) absorption. Steady-state PL quenching of the NPA-CHT (donor) in the presence of acceptor (Ni-CHT nanobioconjugates) is shown in the inset. (b) Picosecond-resolved fluorescence transients of donor (NPA-CHT) and donor-acceptor (NPA-Ni-CHT) complex at 25 °C. The anisotropy decays of the donor (NPA-CHT; symbol: square) and donor-acceptor (NPA-Ni-CHT; symbol: circle) complex are shown in the inset.

band at 417 nm, the details of which are given in the ESI.† As revealed from inset of Fig. 5a the overall steady state emission intensity of the donor emission drastically decreased in the presence of acceptor. Also, the faster decay of the donor in the presence of acceptor (Fig. 5b) as compared to that of the donor alone confirms the energy transfer from NPA to Ni NPs in CHT. Further confirmation of the energy transfer comes from the faster anisotropy decay (inset of Fig. 5b) of the donor NPA (0.11 ns (18%) and 0.98 ns (33%)) in the presence of Ni NPs as compared to that of the donor alone (0.33 ns (28%) and 4.32 ns (40%)).⁵⁶ The calculated (from eqn (S4) and (S5)†) donor to acceptor energy transfer efficiency from steady-state and time-resolved studies is 97.5 and 87.0%, respectively. Control experiments have also been carried out with donor (NPA-CHT) in the presence of nickel ions and the lifetime values of the donor (NPA-CHT) in the absence of the nickel ions have been found to be similar to that of NPA-CHT in the presence of nickel ions. It has to be carefully noted that we have used the amplitude weighted time constants⁵⁷ for the donor in the absence (D) and presence of acceptor (DA) to evaluate the energy transfer efficiency (*E*) using time-resolved data (see ESI for details†). The estimated donor-acceptor distances from steady-state and time-resolved experiments are 17.7 and 28.1 ± 1 Å, respectively. For a well-behaved system, the ratio of the integrated areas under the time-resolved emission decays for donor and

donor/acceptor complex should correlate with the integrated areas under the steady-state emission spectra. In principle, one of the methods can be used to estimate D–A distance. However, due to some possibility of reabsorption of donor emission by the acceptor, there is a disagreement between the estimated donor–acceptor (DA) distances from steady-state and time-resolved studies. In one of our recent studies,⁵⁸ we have reported the potential danger of using steady-state fluorescence quenching to conclude the nature of energy transfer as Förster type and to estimate the DA distances. The globular enzyme CHT has a diameter of 44 Å, and the estimated distance of any surface sites from the catalytic center is less than the diameter of the enzyme. The possible nucleation sites (DA distance of 27.1 Å) for the formation of Ni NPs in CHT could be free amine groups from the amino acid residues or the thiols at the protein surface, which could have been easily generated by the reduction of disulfide bonds by NaBH₄. These functional groups (thiols and amines) have the ability to bind covalently with the nickel particle surface, leading to the formation of nanobioconjugates. After characterising the attachment of Ni NPs to CHT using a FRET technique, which essentially probes the inner subdomain distance between the enzymatic active site (NPA position) and one of protein surface sites (Ni nanoparticle position), we have used the distance as a marker for various temperature-induced folding states of the protein. Proteins would go through various folding states due to temperature change to avoid heat denaturation.^{59,60} Temperature dependent CD spectroscopy on the protein CHT revealed the various folding states at different temperatures. The observed change in the helicity of the protein at 232 nm can be translated to the unfolded fraction with the increase of temperature.⁶¹ As evident from Fig. 6, the transition temperature (T_m , the midpoint of unfolding transition) is at 50 °C. From our FRET studies it is evident that the protein retains its structural integrity to 40 °C. The estimated D–A distances at 20 °C and 40 °C are similar: 28 ± 1 Å and 29 ± 1 Å respectively. However, at 65 °C the average D–A distance is 35.7 ± 1 Å, which is a signature of the perturbation of the protein from its native state. Our observation is consistent with other studies on the protein CHT.⁶²

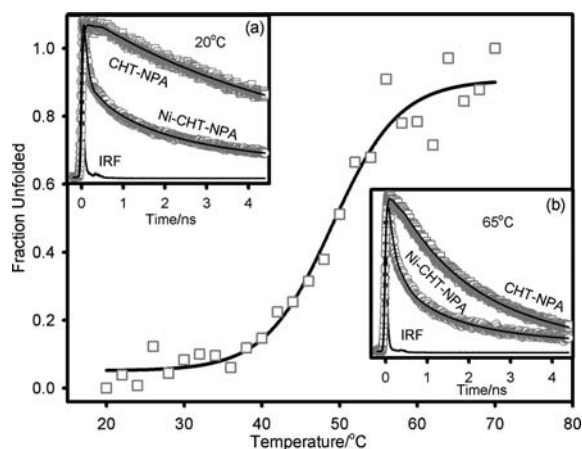


Fig. 6 The thermal unfolding curve of CHT. The transition temperature (T_m , the midpoint of the unfolding transition) is at 50 °C. Picosecond-resolved fluorescence transients of donor (NPA–CHT; symbol: square) and donor–acceptor (NPA–Ni–CHT; symbol: circle) complex at 20 °C and 65 °C are shown in insets (a) and (b) respectively.

Conclusion

In summary, we have prepared luminescent Ni NPs (~2.5 nm) conjugated to a biomolecule CHT, which exhibit superparamagnetism above $T_B = 13.2$ K. We found that the native structure of the protein in the reconstituted Ni–CHT bioconjugates was similar to that of reconstituted CHT. The functional integrity of the Ni–CHT bioconjugates was confirmed by monitoring the enzymatic activities of the reconstituted CHT and reconstituted Ni–CHT bioconjugates by using UV-Vis absorption spectroscopy. FRET studies using a fluorescent probe, NPA bound at the enzymatic active site of CHT, as the donor and Ni NP bound CHT as the acceptor confirmed the conjugation of Ni NPs to CHT. As evidenced from our studies, the methodology would provide a tool for investigations of protein folding/unfolding. The unique properties of these luminescent and magnetic NP bioconjugates, such as visualization by fluorescence and manipulation in magnetic fields, have potential use in labels for living cells and tissues as well as for biomedical assays and as an MRI contrast enhancer. Also, the nanobioconjugates may find application in the field of bionanotechnology as the protein layer provides multiple functional groups (amines, carboxylic acids and cysteine residues) for covalent conjugation with other biological molecules and biocompatible polymers.

Experimental section

Sample preparation

Nickel(II) nitrate hexahydrate ($\text{Ni}(\text{NO}_3)_2 \cdot 6\text{H}_2\text{O}$ > 99.9%), sodium borohydride (NaBH_4 , >99.9%), CHT, NPA, and Ala-Ala-Phe 7-amido-4-methyl coumarin (AAF-AMC) were obtained from Sigma Aldrich. The chemicals and the proteins are of highest commercially available purity and were used as received. All aqueous solutions were prepared using double distilled water from a Millipore system and then degassed by bubbling with dry argon gas for 30 min to control the growth of the NPs as pointed out by Wilcoxon *et al.*⁶³ Since sodium borohydride, catalyzed by metallic ions, can react directly with water to form hydrogen, freshly prepared aqueous solutions of NaBH_4 were used in the experiment. The synthesis of CHT-conjugated Ni NPs was carried out, following the method of Burt *et al.*,⁶⁴ by chemical reduction in the aqueous solution using NaBH_4 as a reducing agent at ambient conditions. A typical procedure for the synthesis of conjugated Ni NPs is as follows: 10 mL of 100 μM CHT aqueous solution was prepared. This was carefully degassed with argon for 30 min. A freshly prepared $\text{Ni}(\text{NO}_3)_2$ solution (100 μL of 1000 mM) was then added to the above protein solution with vigorous stirring. A degassed aqueous NaBH_4 solution (2 M) was then added to the above solution under vigorous stirring. The final molar ratio of $\text{BH}_4^- : \text{Ni}^{2+}$ in the aqueous solution was maintained at 10 : 1. The reaction was allowed to proceed for 3 h, and the final solution was dialyzed against water exhaustively to remove any excess of salts and NaBH_4 left in the solution at 4 °C. The final dialyzed solution was collected and stored at 4 °C prior to analysis. Details of the experimental methodology, including steady-state and time-resolved measurements can be obtained from the ESI.†

Acknowledgements

P.K.V. thanks CSIR (India) and A.G. thanks UGC (India) for a fellowship. We thank the DST for a financial grant (SR/SO/BB-15/2007). Nguyen T.K. Thanh thanks the Royal Society for her Royal Society University Research Fellowship.

Notes and references

- 1 C. M. Niemeyer, *Angew. Chem., Int. Ed.*, 2001, **40**, 4128–4158.
- 2 C. M. Niemeyer, *Angew. Chem., Int. Ed.*, 2003, **42**, 5796–5800.
- 3 W. Shenton, D. Pum, U. B. Sleytr and S. Mann, *Nature*, 1997, **389**, 585–587.
- 4 E. Braun, Y. Eichen, U. Sivan and G. Ben-Yoseph, *Nature*, 1998, **391**, 775–778.
- 5 T. Douglas and M. Young, *Nature*, 1998, **393**, 152–155.
- 6 S. Behrens, K. Rahn, W. Habicht, K.-J. Böhm, H. Rösner, E. Dinjus and E. Unger, *Adv. Mater.*, 2002, **14**, 1621–1625.
- 7 S. Mandal, S. Phadtare and M. Sastry, *Curr. Appl. Phys.*, 2005, **5**, 118–127.
- 8 D. Lee, R. L. Donkers, G. Wang, A. S. Harper and R. W. Murray, *J. Am. Chem. Soc.*, 2004, **126**, 6193–6199.
- 9 S. Chen, R. S. Ingram, M. J. Hostetler, J. J. Pietron, R. W. Murray, T. G. Schaaff, J. T. Khoury, M. M. Alvarez and R. L. Whetten, *Science*, 1998, **280**, 2098–2101.
- 10 C.-W. Lu, Y. Hung, J.-K. Hsiao, M. Yao, T.-H. Chung, Y.-S. Lin, S.-H. Wu, S.-C. Hsu, H.-M. Liu, C.-Y. Mou, C.-S. Yang, D.-M. Huang and Y.-C. Chen, *Nano Lett.*, 2007, **7**, 149–154.
- 11 M. Bruchez, M. Moronne, P. Gin, S. Weiss and A. P. Alivisatos, *Science*, 1998, **281**, 2013–2016.
- 12 W. C. W. Chan, D. J. Maxwell, X. Gao, R. E. Bailey, M. Han and S. Nie, *Curr. Opin. Biotechnol.*, 2002, **13**, 40–46.
- 13 M.-K. So, C. Xu, A. M. Loening, S. S. Gambhir and J. Rao, *Nat. Biotechnol.*, 2006, **24**, 339–343.
- 14 X. Michalet, F. F. Pinaud, L. A. Bentolila, J. M. Tsay, S. Doose, J. J. Li, G. Sundaresan, A. M. Wu, S. S. Gambhir and S. Weiss, *Science*, 2005, **307**, 538–544.
- 15 J. Won, M. Kim, Y.-W. Yi, Y. H. Kim, N. Jung and T. K. Kim, *Science*, 2005, **309**, 121–125.
- 16 Y.-M. Huh, Y.-w. Jun, H.-T. Song, S. Kim, J.-S. Choi, J.-H. Lee, S. Yoon, K.-S. Kim, J.-S. Shin, J.-S. Suh and J. Cheon, *J. Am. Chem. Soc.*, 2005, **127**, 12387–12391.
- 17 R. Weissleder, K. Kelly, E. Y. Sun, T. Shtatland and L. Josephson, *Nat. Biotechnol.*, 2005, **23**, 1418–1423.
- 18 L. T. Lu, L. D. Tung, I. Robinson, D. Ung, B. Tan, J. Long, A. I. Cooper, D. G. Fernig and N. T. K. Thanh, *J. Mater. Chem.*, 2008, **18**, 2453–2458.
- 19 L. T. Lu, L. D. Tung, J. Long, D. G. Fernig and N. T. K. Thanh, *J. Mater. Chem.*, 2009, **19**, 6023–6028.
- 20 A. K. Gupta and M. Gupta, *Biomaterials*, 2005, **26**, 3995–4021.
- 21 H. Gu, P.-L. Ho, K. W. T. Tsang, L. Wang and B. Xu, *J. Am. Chem. Soc.*, 2003, **125**, 15702–15703.
- 22 H. Gu, K. Xu, C. Xu and B. Xu, *Chem. Commun.*, 2006, 941–949.
- 23 S. G. Penn, L. He and M. J. Natan, *Curr. Opin. Chem. Biol.*, 2003, **7**, 609–615.
- 24 A. Hultgren, M. Tanase, C. S. Chen and G. J. Meyer, *J. Appl. Phys.*, 2003, **93**, 7554–7556.
- 25 D. Wang, J. He, N. Rosenzweig and Z. Rosenzweig, *Nano Lett.*, 2004, **4**, 409–413.
- 26 S. T. Selvan, P. K. Patra, C. Y. Ang and J. Y. Ying, *Angew. Chem., Int. Ed.*, 2007, **46**, 2448–2452.
- 27 H. Gu, R. Zheng, X. Zhang and B. Xu, *J. Am. Chem. Soc.*, 2004, **126**, 5664–5665.
- 28 J. Gao, W. Zhang, P. Huang, B. Zhang, X. Zhang and B. Xu, *J. Am. Chem. Soc.*, 2008, **130**, 3710–3711.
- 29 A. Henglein, *J. Phys. Chem.*, 1993, **97**, 5457–5471.
- 30 B. Ghosh, P. Chakraborty, S. Mohapatra, P. A. Kurian, C. Vijayan, P. C. Deshmukh and P. Mazzoldi, *Mater. Lett.*, 2007, **61**, 4512–4515.
- 31 J. Hernández-Torres and A. Mendoza-Galván, *Thin Solid Films*, 2005, **472**, 130–135.
- 32 H. Amekura, H. Kitazawa and N. Kishimoto, *Nucl. Instrum. Methods Phys. Res., Sect. B*, 2004, **222**, 96–104.
- 33 T. Isobe, S. Y. Park, R. A. Weeks and R. A. Zuhr, *J. Non-Cryst. Solids*, 1995, **189**, 173–180.
- 34 O. A. Yeshchenko, I. M. Dmitruk, A. A. Alexeenko and A. M. Dmytruk, *J. Phys. Chem. Solids*, 2008, **69**, 1615–1622.
- 35 G. Mie, *Ann. Phys.*, 1908, **330**, 377.
- 36 E. J. Zeman and G. C. Schatz, *J. Phys. Chem.*, 1987, **91**, 634–643.
- 37 W. T. Doyle, *Phys. Rev.*, 1958, **111**, 1067–1072.
- 38 H. Amekura, Y. Takeda and N. Kishimoto, *Thin Solid Films*, 2004, **464–465**, 268–272.
- 39 V. V. Volkov, Z. L. Wang and B. S. Zou, *Chem. Phys. Lett.*, 2001, **337**, 117–124.
- 40 J. P. Wilcoxon, J. E. Martin and P. Provencio, *J. Chem. Phys.*, 2001, **115**, 998–1007.
- 41 U. Kreibitz and L. Genzel, *Surf. Sci.*, 1985, **156**, 678–700.
- 42 F. C. Fonseca, G. F. Goya and R. F. Jardim, *Phys. Rev. B*, 2002, **66**, 104406.
- 43 A. Roy, V. Srinivas, S. Ram and T. V. C. Rao, *J. Phys.: Condens. Matter*, 2007, **19**, 346220.
- 44 A. Roy, V. Srinivas, S. Ram, J. A. D. Toro and U. Mizutani, *Phys. Rev. B*, 2005, **71**, 184443.
- 45 Y. Hou, J. Yu and S. Gao, *J. Mater. Chem.*, 2003, **13**, 1983–1987.
- 46 J. P. Hennessey and W. C. Johnson, *Biochemistry*, 1981, **20**, 1085–1094.
- 47 B. J. Jordan, R. Hong, B. Gider, J. Hill, T. Emrick and V. M. Rotello, *Soft Matter*, 2006, **2**, 558–560.
- 48 S. S. Narayanan, R. Sarkar and S. K. Pal, *J. Phys. Chem. C*, 2007, **111**, 11539–11543.
- 49 S. S. Narayanan and S. K. Pal, *J. Phys. Chem. C*, 2008, **112**, 4874–4879.
- 50 J. J. Béchet, A. Dupaix, J. Yon, M. Wakselman, J.-C. Robert and M. Vilkas, *Eur. J. Biochem.*, 1973, **35**, 527–539.
- 51 J. W. Chang and R. B. Martin, *J. Phys. Chem.*, 1969, **73**, 4277–4283.
- 52 Q. Fernando and H. Freiser, *J. Am. Chem. Soc.*, 1958, **80**, 4928–4931.
- 53 J. M. White, R. A. Manning and N. C. Li, *J. Am. Chem. Soc.*, 1956, **78**, 2367–2370.
- 54 J. M. Tsangaris, J. W. Chang and R. B. Martin, *Arch. Biochem. Biophys.*, 1969, **130**, 53–58.
- 55 R. P. Haugland and L. Stryer, in *Conformation of Biopolymers*, ed. G. M. Ramachandran, Academic Press, New York, 1967.
- 56 E. K. L. Yeow, K. P. Ghiggino, J. N. H. Reek, M. J. Crossley, A. W. Bosman, A. P. H. J. Schenning and E. W. Meijer, *J. Phys. Chem. B*, 2000, **104**, 2596–2606.
- 57 J. R. Lakowicz, *Principles of Fluorescence Spectroscopy*, Kluwer Academic/Plenum, New York, 1999.
- 58 P. Majumder, R. Sarkar, A. K. Shaw, A. Chakraborty and S. K. Pal, *J. Colloid Interface Sci.*, 2005, **290**, 462–474.
- 59 R. Sarkar, S. S. Narayanan, L.-O. PaÈlsson, F. Dias, A. Monkman and S. K. Pal, *J. Phys. Chem. B*, 2007, **111**, 12294–12298.
- 60 R. K. Mitra, P. K. Verma, D. Wulferding, D. Menzel, T. Mitra, A. M. Todea, P. Lemmens, A. Mueller and S. K. Pal, *ChemPhysChem*, 2010, **11**, 389–393.
- 61 J. K. A. Kamal, T. Xia, S. K. Pal, L. Zhao and A. H. Zewail, *Chem. Phys. Lett.*, 2004, **387**, 209–215.
- 62 D. Banerjee and S. K. Pal, *Langmuir*, 2008, **24**, 8163–8168.
- 63 J. P. Wilcoxon, R. L. Williamson and R. Baughman, *J. Chem. Phys.*, 1993, **98**, 9933–9950.
- 64 J. L. Burt, C. Gutiérrez-Wing, M. Miki-Yoshida and M. José-Yacamán, *Langmuir*, 2004, **20**, 11778–11783.